Chapter 4

Role of Hydrophobic Force in the Thinning of Foam Films Containing Methyl Isobutyl Carbinol

Abstract

The thin film pressure balance (TFPB) technique was used to study the kinetics of film thinning at various concentrations of a nonionic surfactant, methyl isobutyl carbinol (MIBC), in the presence of 0.1 M sodium chloride (NaCl). The experimental data were compared with the predictions from the Reynolds equation to determine the contributions from hydrophobic force to film thinning. Despite the high electrolyte concentration employed, the hydrophobic force was 15 to 90 times stronger than the van der Waals force over the MIBC concentrations investigated. It was found that the hydrophobic force decreased with increasing MIBC concentration, which corroborated well with the changes in film lifetime, foam lifetime, and the critical rupture thickness. On the other hand, both surface tension and film elasticity change little at low surfactant concentrations, particularly at the concentrations where the nonionic surfactant is used for flotation. It is, therefore, suggested that at relatively low MIBC concentrations foams are destabilized by the hydrophobic force, which is dampened by the surfactant.

10.1016/j.colsurfa.2005.10.070

Published on Web 12/15/2005

4.1 Introduction

Bubbles and foams are used widely in a variety of industrial applications, *e.g.*, froth flotation, tertiary oil recovery, foam fractionation, food processing, manufacturing of personal care products, *etc*., and control of bubble size and of foam stability is important in many of these applications. In flotation, for example, small air bubbles are introduced to an aqueous suspension (pulp) containing both hydrophilic and hydrophobic particles so that the latter is collected selectively on the surface of the bubble. The bubbles laden with hydrophobic particles rise to the surface of the pulp, forming a three-phase foam (froth), which is subsequently removed mechanically or by displacement. The rate of flotation increases sharply with decreasing bubble size. Therefore, the bubble size in the pulp phase is reduced by adding (non-ionic) surfactants and increasing energy dissipation for bubble generation, while the bubble size in the froth phase is controlled by adjusting the height of the froth. The importance in controlling froth stability in flotation is widely recognized in recent years (1-3).

Foam is thermodynamically unstable; therefore, bubble size coarsens by coalescence as a means of reducing free energy. The lifetime of foam is controlled by drainage and rupture. For a horizontal foam film, the driving force for the drainage process is the capillary pressure. The drainage stops and the film thickness reaches equilibrium when the capillary pressure becomes equal to the disjoining pressure of the thin film. It is generally recognized that the disjoining pressure is determined by the sum of the attractive van der Waals force and the repulsive double-layer force. Thus, one can determine the contribution from one of the two surface forces to the disjoining pressure by knowing the equilibrium film thickness, capillary pressure, and the contribution from the other surface force. This approach works well at high surfactant concentrations but fails at low concentrations, suggesting that there may be an additional attractive force (*i.e.*, hydrophobic force) playing a role in foam stability (4,5).

As the thickness of a foam film is reduced by drainage, the film ruptures catastrophically when the thickness reaches a critical thickness (H_{cr}). It is generally believed that, a foam film is always in thermally- or mechanically-induced oscillation. The amplitude of the oscillation increases, when the instantaneous distance between the two surfaces is within the range of a significant attractive force such as van der Waals force. When the two surfaces touch each other, the film ruptures. Angarska et al (6) showed that this capillary wave mechanism can predict H_{cr} at high surfactant concentrations in the absence of energy barrier but not at low concentrations. They found that at the low surfactant concentrations the model works better by recognizing the contribution from the hydrophobic force to the rupture mechanism.

The role of hydrophobic force in film thinning has also been studied by the authors of the present communication (7). They measured the kinetics of thinning of horizontal foam films of very small radius (<0.1 mm) and fitted the data to the Reynolds equation (8,9):

$$-\frac{dH}{dt} = \frac{2H^3\Delta P}{3\mu R_f^{\,2}} \qquad [4.1]$$

where H is film thickness, t drainage time, μ dynamic viscosity, R_f is film radius, and ΔP is the driving force for film thinning. The driving force is given by the following relation:

$$\Delta P = P_c - \Pi \qquad [4.2]$$

where the capillary pressure P_c is given by (10)

$$P_c = \frac{2\gamma}{R_c} \qquad [4.3]$$

and the disjoining pressure by

$$\Pi = \Pi_{el} + \Pi_{vw} + \Pi_{hb} \qquad [4.4]$$

In Eqs. [4.3] and [4.4], γ is surface tension and R_c is the radius of the film holder, while Π_{el}, Π_{vw}, and Π_{hb} represent the contributions from the electrostatic, van der Waals and hydrophobic forces, respectively.

In soap films, the first term of Eq. [4.4] is repulsive, while the latter two are attractive. It has been shown that the hydrophobic disjoining pressure can be represented as a power law (4, 11-13):

$$\Pi_{hb} = -\frac{K_{232}}{6\pi H^3} \qquad [4.5]$$

where K_{232} is a constant representing the hydrophobic interaction between two gas phases (or bubbles) **2** interacting with water **3** at a separation distance of H. An advantage of using Eq. [4.5] is that it is of the same form as the van der Waals force:

$$\Pi_{vw} = -\frac{A_{232}}{6\pi H^3} \qquad [4.6]$$

so that one can compare the magnitudes of the hydrophobic force with that of the van der Waals force by means of the two force constants, *i.e.*, K_{232} and A_{232} (Hamaker constant). It was found that K_{232} decreases with increasing concentration of surfactant (SDS) and inorganic electrolyte (NaCl) (5, 7).

In principle, the Reynolds equation is applicable to the foam films with tangentially immobile surfaces. It has been shown that this condition can be met by using very small films stabilized by a surfactant (10, 14, 15). It has also been shown that Eq. [4.1] can be used even at low surfactant concentrations (6, 16).

In the present work, the kinetics of thinning horizontal foam films was studied in the presence of methyl isobutyl carbinol (MIBC). This reagent was chosen because it is one of the most widely used surfactants that are used to produce small air bubbles for flotation. The experiments were conducted in 0.1 M NaCl solutions to suppress the electrical double layer repulsion. This was necessary as there are no reliable methods of determining double-layer potentials, which is necessary in determining Π_{el}. This approach will allow determination of K_{232} without involving the ambiguity associated with determining the double layer potentials. The information obtained in the present work can be useful not only for better understanding foam stability but also for modeling flotation (or bubble-particle attachment) as a hydrophobic interaction (17).

4.2 Materials and Methods

A Nanopure water treatment unit was used to obtain double-distilled and deionized water with a conductivity of 18.2 $M\Omega cm^{-1}$. Methyl Isobutyl Carbinol, MIBC (99%) from Research Chemicals Ltd. was used as received. A high-purity sodium chloride (99.99%) from Alfa Aesar was used as an electrolyte.

The TFPB technique was used to measure the rate of film thinning in a Scheludko cell (9,10). The inner radius of the film holder (R_c) was 2.0 mm. Following the recommendation by Exerowa et al (18), the inner wall of the film holder was scratched with a sharpening stone to improve wettability The cell was placed in a vapor-saturated chamber, which was placed on a tilt stage (M-044.00, Polytec PI), which in turn was placed on an inverted microscopic stage (Olympus IX51). The chamber was water-jacketed to maintain the temperature within 25±0.1°C, and the tilt stage was carefully adjusted before each measurement to obtain horizontal foam films. The fluoresce condenser of the inverted microscope was specially modified so that only a circular zone of 0.045 mm radius of the film was illuminated. A PC-based data acquisition system was used to record the intensities of the reflected lights, from which film thicknesses were obtained using the microinterferometric technique (9). The film radii (R_f) were controlled within the 0.060-0.070 mm range. According to Radoev et al (19), the nonhomogeneity of film thickness across the film (H_{max}-H_{min}) approaches zero when film radius is below 0.1 mm. These conditions were necessary to minimize the influence from hydrodynamic or thermal fluctuations, so that the Reynolds equation (Eq. [4.1]) can be used to analyze the rate of film thinning. Further discussion on the validity of this method is given in the Discussion section.

The stability of three-dimensional foams was measured by shake tests (20). The tests were conducted using 50 ml volumetric flasks, each containing 25 ml of a surfactant solution. In each test, a flask was hand shaken 20 times at a fixed frequency and then left to stand for observation. After a few seconds, a clear surface began to appear at the center of the foam. As the time elapses, the clear surface expanded toward the wall of the flask, forming a ring of bubbles, which subsequently broke into clusters of bubbles. The size of clusters was reduced with time, some of which eventually becoming isolated bubbles. The time it took until only the isolated bubbles became visible was taken as a measure of foam stability.

4.3 Results

Figure 4.1 shows the film thickness (H) versus time (t) plots obtained at three different concentrations of MIBC in the presence of 0.1 M NaCl. At such a high electrolyte concentration, the electrostatic double layer force was effectively screened so that $\Pi_{el} \approx 0$, and as a consequence the films became unstable. The film ruptured in 5.7 s at H=63.3 nm at 10^{-5} M MIBC. At 3×10^{-3} M MIBC, the film became more stable, with the rupture occurring in 14.4 s at 26.1 nm. At 3×10^{-2} M MIBC, the film lasted as long as 26.3 s, with the rupture thickness of 31.3 nm. On the other hand, the experimental results obtained under the condition of $\Pi_{el} \approx 0$ made it possible to determine the contributions from the hydrophobic force unambiguously. At low ionic strengths, the magnitudes of hydrophobic force have a degree of uncertainties associated with the values of $\Pi \neq 0$ (6, 7).

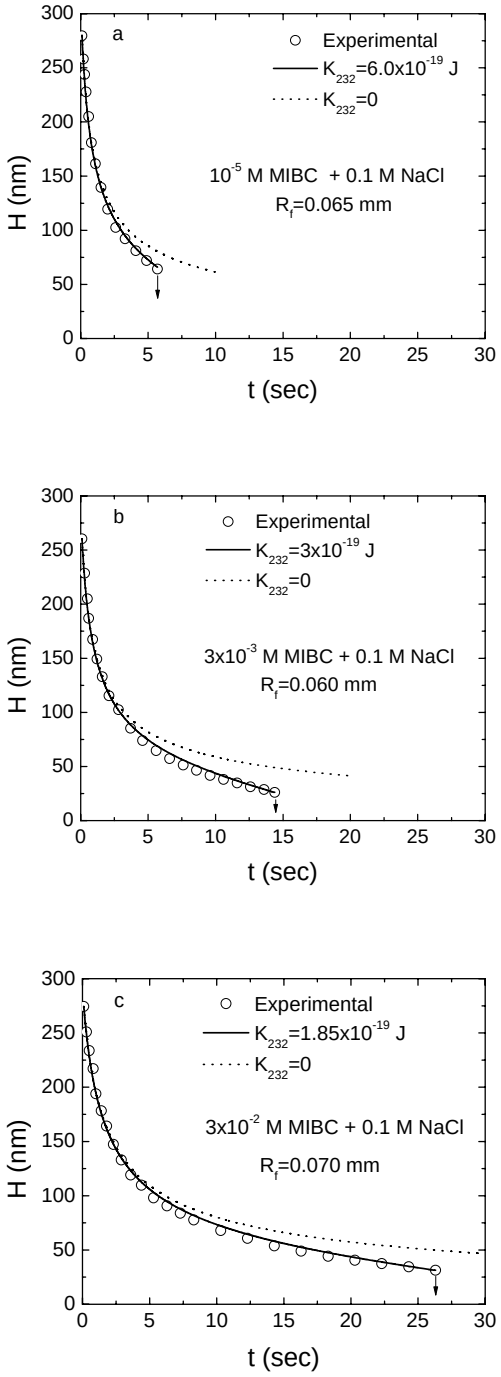

Figure 4.1 Kinetics of film thinning at a) 10^{-5} M MIBC and 0.1 M NaCl; b) 3×10^{-3} M MIBC and 0.1 M NaCl; c) 3×10^{-2} M MIBC and 0.1 M NaCl. The solid lines represent the Reynolds equation (Eq. [4.1]) by considering contributions from the hydrophobic force with fitted values of K_{232}. The contributions from double-layer force are set to 0, while those from the van der Waals force were calculated using the Hamaker constant obtained using the Lifshitz theory (Eq. [4.9]).

Along with the experimental data, Figure 4.1 shows the Reynolds equation (Eq. [4.1]) plotted using the driving forces (ΔP) calculated using Eq. [4.2] with and without considering the hydrophobic force. In using Eq. [4.1], the capillary pressure (P_c) was calculated from the surface tension (γ) data of Comley et al (21) using Eq. [4.3], while the disjoining pressure (Π) was calculated using Eq. [4.4]. In using Eq. [4.1], the viscosity (μ) was set to be equal to that of water (0.900 cP at 25 °C) (22).

It was shown that Eq. [4.4] can be written as (7):

$$\begin{aligned}\Pi &= \Pi_{el} + \Pi_{vw} + \Pi_{hb} \\ &= 64 C_{el} \mathrm{R} T \tanh^2\left(\frac{ze\psi_s}{4kT}\right)\exp(-\kappa H) - \frac{A_{232}}{6\pi H^3} - \frac{K_{232}}{6\pi H^3}\end{aligned} \quad [4.7]$$

where C_{el} is electrolyte concentration, R the gas constant, T the absolute temperature, z ionic valency, e the electronic charge, ψ_s surface potential, k the Boltzmann's constant, and κ the inverse Debye length. At 0.1 M NaCl, the first term of Eq. [4.7] can be ignored to obtain:

$$\Pi = -\frac{1}{6\pi H^3}[A_{232}(H) + K_{232}] \quad [4.8]$$

In the present work, the Hamaker constants, A_{232}, were calculated using the following equation (23, 24):

$$A_{232}(H) = \frac{3}{4}kT\left(\frac{\varepsilon_2 - \varepsilon_3}{\varepsilon_2 + \varepsilon_3}\right)^2 (2\kappa H)e^{-2\kappa H} + \frac{3h_P\nu_e}{16\sqrt{2}}\frac{(n_2^2 - n_3^2)^2}{(n_2^2 + n_3^2)^{3/2}}\mathrm{F}(\widetilde{H}) \quad [4.9]$$

in which $\widetilde{H}$ is the dimensionless distance, given by

$$\widetilde{H} = n_3(n_2^2 + n_3^2)^{1/2}\frac{2\pi\nu_e H}{c} \quad [4.10]$$

and

$$\mathrm{F}(\widetilde{H}) \approx (1 + (\frac{\pi\widetilde{H}}{4\sqrt{2}})^{3/2})^{-2/3} \quad [4.11]$$

where h_P is the Planck's constant (6.63×10^{-34} J·s), ν_e the main electronic adsorption frequency (3×10^{15} Hz), c the speed of light in vacuum (3.0×10^{8} m/s), n_2 the refractive index of air, n_3 the refractive index of solution, ε_2 the dielectric constant of air, and ε_3 is the dielectric constant of water. At a high electrolyte concentration (e.g., 0.1 M NaCl), the first term of Eq. [4.9] may be neglected.

The values of A_{232} were calculated using Eq. [4.9] at the critical rupture thicknesses measured in the present work and are plotted in Figure 4.2. Also shown in this figure are the values of the hydrophobic force constants, K_{232}, obtained by fitting the film thinning kinetics data obtained in the present work (*e.g.*, Figure 4.1) to the Reynolds equation (Eq. [4.1]). In Figure 4.1, the dotted curves represent Eq. [4.1] without considering the hydrophobic force, *i.e.*, K_{232}=0, while the solid lines represent the equation with $K_{232}=6\times10^{-19}$ J at 10^{-5} M MIBC; $K_{232}=3\times10^{-19}$ J at 3×10^{-3} M MIBC; and $K_{232}=1.85\times10^{-19}$ J at 3×10^{-2} M MIBC. As shown in Figure 4.2, the K_{232} values determined from the curve fitting procedure were approximately 15 to 90 times larger than the Hamaker constants calculated using Eq. [4.9] at the critical film rupture thicknesses (H_{cr}).

At $H>H_{cr}$, the difference between K_{232} and A_{232} should be even larger than shown in Figure 4.2, because the retardation effect causes the van der Waals force to decrease with increasing film thickness. In the present work, the hydrophobic force is represented in the same form as the van der Waals force, which makes it possible to directly compare the two by means of K_{232} and A_{232}. That the former is substantially larger than the latter even at a very high electrolyte concentration suggests that the hydrophobic force is real.

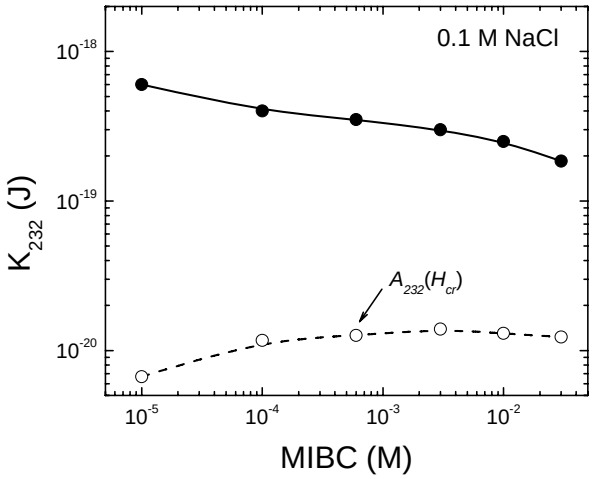

Figure 4.2 Effect of MIBC concentration on K_{232} at 0.1 M NaCl. The results were obtained by fitting the film thinning data to the Reynolds equation (Eq. [4.1]). The Hamaker constants (A_{232}) at the critical rupture thicknesses were calculated using the Lifshitz theory (Equation [4.9]) by considering the retardation effect.

In Figure 4.3, the K_{232} values given Figure 4.2 are replotted along with the lifetimes of the single foam films (film lifetime) and the lifetimes of the three-dimensional foams (foam lifetime) determined at different MIBC concentrations. The film lifetime represents the time elapsed prior to the rupture of single foam films, while the foam lifetime represents the time it took for a three-dimensional foam to become single bubbles in the shake tests. As shown, an increase in MIBC concentration caused both the film lifetime and the foam life time to increase, which corroborates well with the changes in K_{232}.

According to Eqs. [4.1] to [4.3], capillary pressure and, hence, the driving force (ΔP) for film thinning decreases with decreasing surface tension. Therefore, the decrease in surface tension should also be responsible for the increase in the film lifetime and the foam lifetime shown in Figure 4.3. At low surfactant concentrations, however, the change in surface tension is minimal, as depicted by the dashed line representing the Langmuir-Szyszkowski equation:

$$\gamma = \gamma_0 - RT\Gamma_m \ln(1 + K_L c) \qquad [4.12]$$

that has been fitted to the surface tension data of Comley et al (21) given in Figure 4.3. In the above equation, γ_0 is the surface tension of pure water, Γ_m (=5x10^{-6} mol/m^2) the monolayer coverage, K_L (=230 M^{-1}) the equilibrium constant, and c is the bulk MIBC concentration. Thus, the data presented in Figure 4.3 show that at low surfactant concentrations both the single foam film and the three dimensional foam are destabilized by hydrophobic force, while at high surfactant concentrations they are stabilized by surface tension lowering.

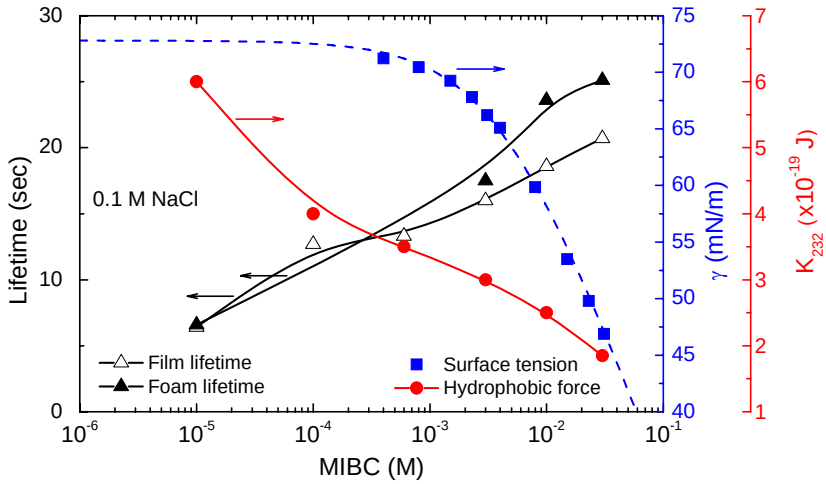

Figure 4.3 Effect of MIBC concentration at 0.1 M NaCl on the lifetimes of foam (▲) and film (Δ). The surface tension data (■) are from Comley et al (21), and the dashed line represents the best fit of the surface tension data using the Langmuir-Szyszkowski equation (Eq. [4.12]). Both the film and foam lifetimes increased with decreasing hydrophobic force constant K_{232} (●). The K_{232} values were calculated from the film thinning data using the Reynolds equation (Eq. [4.1]).

Figure 4.4 shows the effect of MIBC concentration on the critical rupture thicknesses (H_{cr}) measured at 0.1 M NaCl. Vrij (25) and Vrij and Overbeek (26) derived a predictive model for H_{cr}:

$$H_{cr} \approx 0.207\left(\frac{A_{232}^{\,2} R_f^{\,2}}{\gamma P_c}\right)^{1/7} \qquad [4.13]$$

based on the capillary wave mechanism. Eq. [4.13] is applicable when $|\Pi_{vw}| << P_c$, a condition that is applicable for the measurements conducted in the present work, particularly at low MIBC concentrations. The film radii (R_f) were controlled within the 0.060-0.070 mm range. Therefore, H_{cr} should vary primarily with A_{232} and γ according to Eq. [4.13]. For this reason, Figure 4.4 also shows the changes in A_{232}, K_{232}, and γ with MIBC concentration. It is interesting to note that A_{232} varies little, while K_{232} decreases sharply at the low concentration range where H_{cr} decreases sharply. It may be concluded,

therefore, that the decrease in H_{cr} at low concentration range is largely due to the dampening of the hydrophobic force by the surfactant. According to Eq. [4.13], H_{cr} should also vary with surface tension, which, however, changes little at the low concentration range. Therefore, the sharp decrease in H_{cr} cannot be attributed to the change in surface tension.

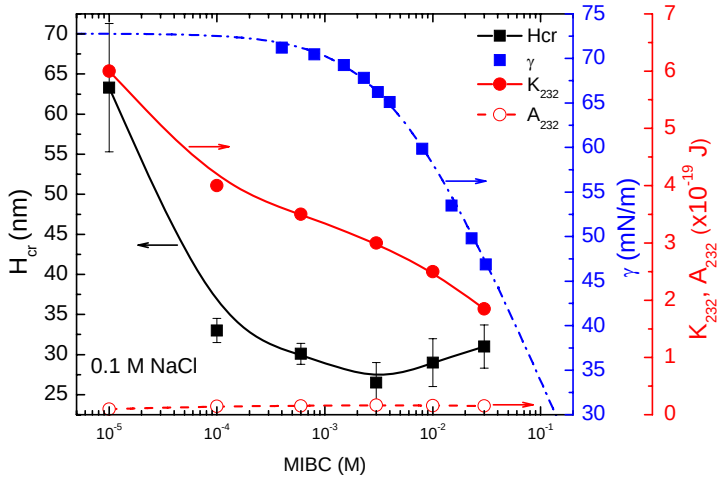

Figure 4.4 Effect of MIBC concentration on the critical rupture thickness (H_{cr}). The surface tension data (■) were from Comley et al (21), and the dash-dotted line represents the best fit of the surface tension data to the Langmuir-Szyszkowski equation (Eq. [4.12]). The K_{232} values (●) were obtained by fitting the film thinning kinetics data to the Reynolds equation (Eq. [4.1]). The Hamaker constants at H_{cr} (○) were calculated using the Lifshiz theory (Eq. [4.9]) by considering the retardation effect.

Note also that H_{cr} starts to increase after reaching a minimum (26.5 nm) at $3x10^{-3}$ M MIBC. Similar observations were also made with sodium dodecylsulfate (SDS) near its CMC by other investigators (27, 28). The increase in H_{cr} above $3x10^{-3}$ M MIBC can be attributed to the surface tension decrease, which was more significant than the decrease in K_{232}.

It is well known that the stability of foams and foam films is determined not only by surface forces (or disjoining pressures) but also by film elasticities (14, 29, 30). Therefore, the film lifetimes and foam lifetimes measured in the present work have been replotted in Figure 4.5 as functions of MIBC concentration, and compared with film elasticities (E). Gibbs defined film elasticity as follows:

$$E = \frac{2d\gamma}{d\ln A} \qquad [4.14]$$

where A is the film surface area. Equation [4.14] can be rewritten as follows:

$$E = 2A\frac{d\gamma}{dA} = 2A\frac{d\gamma}{dc}\frac{dc}{dA} \qquad [4.15]$$

where c is the bulk surfactant concentration. For a closed system, the volume of a foam film, $V = AH$, is constant, *i.e.*, dV=0, where H is film thickness. Also, the total number of the surfactant molecules is constant in a closed system. Therefore,

$$d(2A\Gamma + Vc) = 0 \qquad [4.16]$$

which gives

$$dc = -\frac{2(\Gamma dA + Ad\Gamma)}{AH} \qquad [4.17]$$

under conditions of constant volume. Eq. [4.17] is similar to Christenson and Yaminsky's model (31), except that these authors ignored the $Ad\Gamma$ term, which makes their model applicable only at very high concentrations of surfactant (or electrolyte).

Equation [4.17] can be rewritten as

$$\frac{dc}{dA} = -\frac{2\Gamma}{A(H + 2d\Gamma/dc)} \qquad [4.18]$$

while Gibbs equation gives:

$$\frac{d\gamma}{dc} = -\frac{RT\Gamma}{c} \qquad [4.19]$$

Substituting Eqs. [4.18] and [4.19] into Eq. [4.15], one obtains an expression for the Gibbs elasticity as follows:

$$E = \frac{4RT\Gamma^2}{c(H + 2d\Gamma/dc)} \qquad [4.20]$$

Equation [4.20] can be transformed into a more useful form by combining it with the Langmuir isotherm:

$$\Gamma = \frac{\Gamma_m K_L c}{1 + K_L c} \qquad [4.21]$$

which can be differentiated to obtain:

$$\frac{d\Gamma}{dc} = \frac{\Gamma_m K_L}{(1 + K_L c)^2} \qquad [4.22]$$

Substituting Eqs. [4.21] and [4.22] into Eq. [4.20] gives a useful expression for Gibbs elasticity:

$$E = \frac{4cRT\Gamma_m{}^2 K_L{}^2}{H(1 + K_L c)^2 + 2\Gamma_m K_L} \qquad [4.23]$$

In the present work, the values of Gibbs elasticities (E) have been calculated using Eq. [4.23], in which H was set equal to the measured critical rupture thicknesses (H_{cr}) and

the values of Γ_m and K_L were obtained by fitting the surface tension data to the Langmuir-Szyszkowski equation (Eq. [4.12]). The results are shown in Figure 4.5 (as a solid line) along with the film lifetimes and the foam lifetimes measured in the present work. As shown, the film elasticity increases with increasing MIBC concentration, reaching a maximum at 4×10^{-2} M. The film and foam lifetimes also increase accordingly. At low concentrations (below 10^{-3} M), however, the increase is relatively small. Therefore, the increase in film stability in this concentration region is largely due to the decrease in K_{232}.

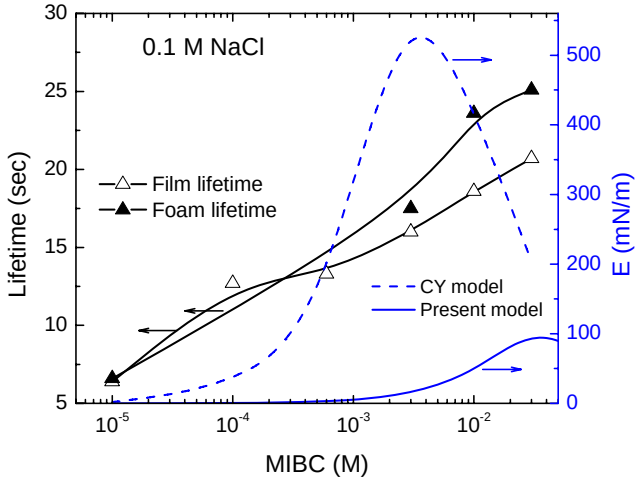

Figure 4.5 Effect of film elasticity (E) on the film lifetime (Δ) and the foam lifetime (▲) at various concentrations of MIBC at 0.1 M NaCl. At low surfactant concentrations, the film elasticities calculated using Eq. [4.23] (solid line) may be too small to affect the film and foam stabilities. The film elasticities calculated using the Christenson and Yaminsky's model (31) (dashed line), are higher because of the simplifying assumption involved in its derivation.

Also shown in Figure 4.5 is a plot of Gibbs elasticities (dashed line) calculated as a function of MIBC concentration using the Christenson and Yaminsky's model (31), *i.e.*, Eq. [4.20] without the $d\Gamma/dc$ term. Because this term is in the denominator, their model over predicts the elasticity.

4.4 Discussion

In the present work, the kinetics of film thinning has been studied in the presence of MIBC, the most widely used frothing agent in the mining industry. It is not the most powerful frother but is of low cost and gives brittle froths. In flotation, it is important to have small air bubbles to achieve high collision efficiencies in the pulp phase and to have high surface area flux in the froth phase. On the other hand, excessively stable froth can cause multitudes of problems (*e.g.*, in pumping and setting) downstream. The overfrothing problems become worse in the presence of ultrafine hydrophobic particles that can further increase froth stability. Further, most of the frothers used in flotation are nonionic frothers, because ionic surfactants can adsorb on unwanted mineral components

and float them inadvertently, causing the flotation process nonselective. Thus, MIBC is an ideal frother in that it can produce small air bubbles without creating the overfrothing (*i.e.*, excessively stable froth) problems.

The amount of MIBC used in the flotation industry are usually in the range of 0.5-1.5x10^{-4} M, where the foam film elsticities (E) are in the range of 1-2 mN/m as shown in Figure 4.5. At such low concentrations and low elasticities, bubbles and foams are barely stable but remain hydrophobic. The values of the hydrophobicity constants, K_{232}, determined at 0.1 M NaCl are in the range of 3.7-4.5x10^{-19} J and allow hydrophobic particles to be attracted *via* hydrophobic interaction. These values are more than 30 times larger than the Hamaker constant, A_{232}. The difference between K_{232} and A_{232} should be substantially larger in the absence of electrolyte. At higher MIBC concentrations, the hydrophobic force decreases further, making the hydrophobic interaction less likely. It is well known that excessive frothers are detrimental to flotation (32).

The results obtained in the present work show that air bubbles are most hydrophobic in the absence of MIBC, and its hydrophobicity decreases with increasing concentration of the surfactant. This finding is supported by thermodynamic considerations. As the MIBC concentration is increased, the interfacial tension between air bubble (a hole in water) and water decreases. The questions remain as to whether the hydrophobic forces measured in the present work are real and what the origin(s) is (are). In the present work, the hydrophobic forces were determined in the presence of 0.1 M NaCl, which effectively suppressed the double-layer force. Previously, the magnitudes of the hydrophobic forces at air/water interfaces were estimated using ionic surfactants (4, 5). The use of ionic surfactants made it possible to determine the surface potentials at the air/water interface and to use the extended DLVO theory (Eq. [4.4]) to calculate the contributions from Π_{hb}. However, there is a degree of uncertainties in determining the surface potentials despite the various precautions and corrections. In the present work, however, the kinetics of film thinning was studied under conditions of $\Pi_{el} \approx 0$. Therefore, the hydrophobic forces determined in the present work may be considered real.

It would be of interest to compare the strengths of the hydrophobic forces determined in the present work using TFPB technique to those of the hydrophobic forces measured between hydrophobic solid surfaces (33, 34). By substituting the K_{232} values determined in the present work to the power law:

$$F / R = -\frac{K_{232}}{6H^2} \qquad [4.24]$$

one can calculate the hydrophobic force (F) at a given separation distance (H). In Eq. [4.24], R is the radius of curvature of the macroscopic surfaces used in force measurement. At K_{232} = 6x10^{-19} J, which was the largest hydrophobic force constant obtained in the present work, F/R = -1.0 mN/m at H = 10 nm. This value is similar to F/R = -1.9 and -1.3 mN/m, which were obtained between the silica surfaces coated with octadecyltrimethylammonium chloride (C_{18}TACl) and the mica surfaces coated with dimethyldioctadecylammonium bromide (DDOA), respectively.

Accepting that the hydrophobic forces exist at the air/water interface, the results presented in the forgoing section show that the role of MIBC is to dampen the hydrophobic forces at the air bubble/water interfaces and stabilize the bubbles. The

increase in film elasticity should also help stabilizing bubbles, but the dampening of hydrophobic force may be more important in the range of MIBC concentrations where flotation is carried out in practice. Film elasticity becomes important at higher MIBC concentration (*e.g.*, $>10^{-3}$ M).

In general, film stability is controlled by thinning and rupture. A liquid film is thinned to a critical thickness by drainage and reaches an equilibrium thickness when capillary pressure equals the disjoining pressure. The air-water interfaces are subjected to mechanical or thermal oscillation, causing the instantaneous distance between the two interfaces smaller than the measured distance. The instantaneous distance can be within the range of significant van der Waals force and rupture, in which case there may be no need to invoke the hydrophobic force. Many investigators showed indeed that the capillary wave model can predict the critical rupture thicknesses (H_{cr}) in the absence of repulsive forces (6, 19, 24, 25, 35). For example, Angarska el al (6) showed that the model fits well with Manev el al's experimental data (36) obtained at $4.3\text{x}10^{-4}$ M SDS and 0.25 M NaCl. It is not surprising, however, that hydrophobic force does not play a role under such high surfactant and electrolyte conditions, because the air/water interface becomes hydrophilic. At lower SDS concentrations (*i.e.*, $0.5\text{-}1.0\text{x}10^{-6}$ M and 0.3 M NaCl), however, it was necessary for these authors to invoke the hydrophobic force to fit the experimental data.

In the present work, the Reynolds lubrication theory (Eq. [4.1]) was used to determine the contributions to the disjoining pressure from the hydrophobic forces. Since the equation was derived for two solid surfaces interacting in a fluid under no-slip conditions, it should in principle apply only for the liquids sandwiched by tangentially immobile surfactant layers. In this regard, Radoev et al (37) and Ivanov et al (38) developed a method of correcting the Reynolds film thinning velocities (V_{Re}) for diffusion and surface mobility. Angarska et al (6) showed, however, that no corrections were necessary in predicting H_{cr} for the aqueous solutions of $0.5\text{-}10\text{x}10^{-6}$ M SDS in the presence of 0.3 M NaCl. Also, Ivanov et al (16) noted that "even minor surfactant concentration (corresponding to Gibbs elasticity, $E_G \approx 1$ mN/m) is sufficient to suppress almost entirely the surface mobility. He noted further that "above this concentration the effect of the surfactant on the film lifetime and on the foam or emulsion stability is entirely controlled by the disjoining pressure." The foam films studied in the present work in the presence of 10^{-5} to $3\text{x}10^{-2}$ M MIBC showed the Gibbs elasticities that were close to those of the films stabilized in the presence of $5\text{x}10^{-7}$ to 10^{-4} M SDS and 0.3 M NaCl. Therefore, it would be justifiable to use the Reynolds equation without corrections in studying the kinetics of thinning the MIBC-stabilized films and use the results for estimating the magnitudes of the hydrophobic forces.

It has been shown that the hydrophobic force constant, K_{232}, decreases with increasing MIBC concentration, which suggests that the decrease in hydrophobic force may be related to the adsorption of the surfactant at the air/water interface. Figure 4.6 shows a plot of the inverse surface excess (Γ_s^{-1}) of MIBC as determined from Gibbs adsorption isotherm. One can see that K_{232} increases with increasing Γ_s^{-1}, suggesting that the lower the area of the adsorption density is, the stronger the hydrophobic force becomes. That is, the pristine air/water interface is most hydrophobic, and its hydrophobicity and, hence, its hydrophobic force decreases with the surfactant adsorption.

The isotherm has two distinct zones. In zone I, a close-packed monolayer of MIBC is formed at the air/water interface, causing a precipitous increase in K_{232} with increasing Γ_s^{-1}. In Zone II, the surfactant adsorption is significant but they are not well ordered. According to Eriksson and Ljunggren (39), however, the surfactant may adsorb as clusters (or hemimicelles) as a means of minimizing free energy. The results obtained with MIBC are similar to those obtained with SDS in the absence of NaCl (7).

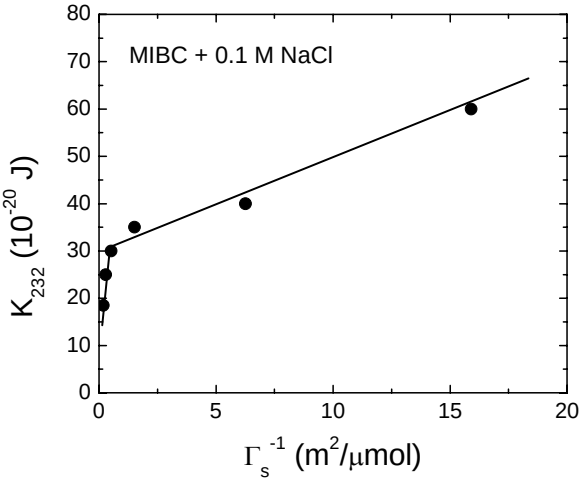

Figure 4.6 The hydrophobic force constants, K_{232}, determined from the film thinning data, are plotted as a function of Γ_s^{-1}. The hydrophobic force decreases sharply as a close-packed monolayer is formed at the air-water interface.

Meyer et al (40) proposed that the very long-range hydrophobic forces measured between two macroscopic surfaces of solids coated with long-chain surfactants might be of electrostatic origin. In the present work, however, the hydrophobic force was observed at 0.1 M NaCl, which makes it difficult to trace its origin to electrostatic attraction. An alternative would be to consider a molecular origin. The free energy gained from the hydrogen bonding of water molecules is much larger than the energy of interaction between water and hydrophobic surfaces. This should cause the water film tension to diminish as the thickness shrinks, which may by manifested as an attractive hydrophobic force. A question remains then as to how the hydrophobic force decays with the distance separating two macroscopic particles. Laskowski and Kitchener (41) suggested that "the multimolecular water layer on the surface of a hydrophobized silica is unstable, which is ascribed to a less favorable state of molecular association at a certain distance from the surface than in normal (bulk) water". These investigators were the first to recognize the existence of a long-range non-DLVO hydrophobic force and to suggest that the long-range character arises from the structural properties of water.

More recently, Eriksson and Yoon (42) integrated the experimental disjoining pressure isotherms obtained at different temperatures by Tsao et al (43), and showed that the excess film entropies ($\Delta S^{f,ex}$) were negative and that their negativity increased with the decreasing distance separating two hydrophobic surfaces. This finding suggests that water is more structured in the intervening layer, which may also be supported by the

sum-frequency (SF) spectra of the water on hydrophobic surfaces. Du et al (44) showed that the SF spectra of the interfacial water on the silica surfaces coated with octadecyltrichlorosilane (OTS) were similar to that of ice. Also, the water on the OTS-coated silica surface showed a prominent peak at 3,700 cm^{-1}, which is due to the dangling (or free) OH groups oriented at the interface. This peak, which is considered as a signature of hydrophobicity, was also observed at the air/water and air/hexane interfaces. Thus, the SF spectra provide evidence that an air bubble in water should be considered a hydrophobic substrate.

4.5 Conclusions

The role of surface forces in film thinning was studied by measuring the kinetics of film thinning at varying concentrations of MIBC and comparing the results with the predictions from the Reynolds lubrication theory. The experiments were conducted using very small foam films produced in a Scheludko cell. The experiments were conducted in 0.1 M NaCl solutions to suppress the double-layer force. Under these conditions, it was possible to fit the Reynolds equation to the experiment by considering the contribution from hydrophobic force to film thinning. The hydrophobic force decreased with increasing MIBC concentration, providing an explanation for the increase in the film lifetime and the foam lifetime observed in the present work. The change in hydrophobic force with MIBC concentration also provides an explanation for the decrease in critical rupture thickness. In the range of the MIBC concentrations (10^{-5} to $3x10^{-2}$ M) investigated, the hydrophobic force constants (K_{232}) were 15 to 90 times larger than the Hamaker constants (A_{232}) calculated using the Lifshitz van der Waals theory by considering the retardation effect. At higher surfactant concentrations, the changes in film elasticity may play a more important role than the hydrophobic force. The K_{232} values determined in the present work vary linearly with the inverse adsorption density (Γ_s^{-1}) of the surfactant, indicating that the hydrophobic force is dampened by the surfactant adsorption.

4.6 References

1. Neethling, S.J., Cilliers, J.J., *Int. J. Miner. Process*. 72 (2003) 267.
2. Ata, S., Ahmed, N., Jameson, G. J., *Int. J. Miner. Process*. 72 (2003) 255.
3. Mathe, Z.T., Harris, M.C., O'Connor, C.T., Franzidis, J-P., *Minerals Engineering* 11 (1998) 397.
4. Yoon, R.-H., Aksoy, B. S., *J Colloid Interface Sci*. 211 (1999) 1.
5. Wang, L., Yoon, R.-H., *Langmuir* 20 (2004) 11457.
6. Angarska, J.K., Dimitrova, B.S., Danov, K.D., Kralchevsky, P.A., Ananthapadmanabhan, K.P., Lips, A., *Langmuir* 20 (2004) 1799.
7. Wang, L., Yoon, R.-H., *Colloids Surfaces A: Physicochem. Eng. Aspects* 263 (2005) 267.
8. Scheludko, A., Platikanov, D., *Kolloid Z*. 175 (1961) 150.
9. Scheludko, A., *Advances in Colloid and Interf. Sci.* 1 (1967**)** 391.

10. Exerowa, D., Kruglyakov, P. M., *Foam and Foam Films*, Elsevier, 1998.

11. Rabinovich, Y.I., Yoon, R.-H., *Langmuir* 10 (1994) 1903.

12. Claesson, P.M., Blom, C.E., Herder, P.C., Ninham, B.W., *J. Colloid Interf. Sci.* 114 (1986) 234.

13. Rabinovich Y. I., and Derjaguin, B. V., *Colloids Surfs.* 30 (1988) 243.

14. Langevin, D., *Advances in Colloid and Interf. Sci.* 88 (2000) 209.

15. Coons, J.E., Halley, P.J., McGlashan, S.A., Tran-Cong, T., *Colloids Surf. A: Physicochem. Eng. Aspects*, 263 (2005) 197.

16. Ivanov, I.B., Danov, K.D., Ananthapadmanabhan, K. P., Lips, A., *Adv. Colloid Interf. Sci.* 114– 115 (2005) 61.

17. Yoon R.-H., and Mao, L., *J Colloid Interface Sci*. 181 (1996) 613.

18. Exerowa, D., Zacharieva, M., Cohen, R., and Platikanov, D., *Colloid Polym. Sci.* 257 (1979) 1089.

19. Radoev, B. P., Scheludko, A. D., Manev, E. D., *J. Colloid Interf. Sci*., 95 (1983) 255.

20. Waltermo, Å., Claesson, P. M., Simonsson, S., Manev, E., Johansson, I., Bergeron, V., *Langmuir* 12 (1996**)** 5271.

21. Comley, B.A., Harris, P.J., Bradshaw, D.J., Harris, M.C., *Int. J. Miner. Process*. 64 (2002) 81.

22. Lide, D. R., and Kehiaian, H. V., *CRC handbook of thermophysical and thermochemical Data*, CRC Press, Boca Raton, FL. 1994.

23. Russel, W.B., Saville, D.A., and Schowalter, W.R., *Colloidal Dispersions.* Cambridge University Press, Cambridge, 1989.

24. Israelachvili, J.N., *Intermolecular and Surface Forces*. Academic Press, London, 1992.

25. Vrij, A., *Discuss. Faraday Soc*. 42 (1966) 23.

26. Vrij, A., Overbeek, J. Th. G., *J. Am. Chem. Soc*. 90 (1968) 3074.

27. Rao, A.A., Wasan, D.T., Manev, E.D., *Chem. Eng. Commun*. 15 (1982) 63.

28. Malhotra, A.K., Wasan, D.T., in: I.B. Ivanov (ed.), *Thin Liquid Films*, surfactant science series, volume 29, 1988, pp829.

29. Fruhner, H., Wantke, K.-D., Lunkenheimer, K., *Colloids Surf. A: Physicochem. Eng. Aspects*,162 (2000)193.

30. Stubenrauch, C., Miller, R., *J. Phys. Chem. B*, 108 (2004) 6412.

31. Christenson, H.K., Yaminsky, V. V., *J. Phys. Chem*. 99 (1995) 10420.

32. Klimpel R.R. and Hansen, R.D., in: P. Somasundaran and B.M. Moudgil (eds.), *Reagents in Mineral Technology*, surfactant science series, Vol. 27, Marcel Dekker, New York and Basel, 1987, 395 pp.

33. Claesson, P.M., Christenson, H.K., *J.Phys. Chem*. 92 (1988) 1650.

34. Zhang, J., Yoon, R.-H., Mao, M., Ducker, W.A., *Langmuir* 21 (2005) 5831.

35. Valkovska, D.S., Danov, K.D., Ivanov, I.B., *Adv. Colloid Interf. Sci*. 96 (2002) 101.

36. Manev, E.D., Sazdanova, S.V., Wasan, D.T., *J. Colloid Interf. Sci*. 97 (1984) 591.

37. Radoev, B.P., Dimitrov, D.S., Ivanov, I.B., *Colloid Polym. Sci*., 252 (1974) 50.

38. Ivanov, I.B., Dimitrov, D.S., Radoev, B.P., *J. Colloid Interf. Sci.*, 63 (1978) 166.

39. Eriksson, J. C., Ljunggren, S., *Colloids Surfs*. 38 (1989) 179.

40. Meyer, E.E., Lin, Q., Hassenkam, T., Oroudjev, E., Israelachvili, J.N., *Proceedings of the National Academy of Sciences* 102 (2005) 6839.

41. Laskowski, J.; Kitchener, J. A. *J. Colloid Interf. Sci*. 30 (1969) 391.

42. Eriksson, J.C., Yoon, R.-H., in: M.C. Fuerstenau (ed.), Society of Mining Engineers, Golden Colorado, in press.

43. Tsao, Y., Yang, S. X., Evans, D. F., Wennerström, H., *Langmuir* 7 (1991) 3154.

44. Du, Q., Freysz, E. and Shen, Y.R., *Science* 264 (1994) 826.